ChemPubSoc Europe

DOI: 10.1002/ejic.201901206

EurJIC European Journal of Inorganic Chemistry

Full Paper

Phosphors

Synthesis of $RE_{6-x}Ca_{1.5x}Si_{11}N_{20}O$ (RE = Yb, Lu; $x \approx 2.2$) with $Lu_{6-x}Ca_{1.5x}Si_{11}N_{20}O:Ce^{3+}$ Offering Interesting Spectral Properties for Yellow-Emitting Phosphors in 1pcLEDs

Lisa Gamperl,[a] Georg Krach,[a] Peter J. Schmidt,[b] and Wolfgang Schnick*[a]

Abstract: The oxonitridosilicates $RE_{6-x}Ca_{1.5x}Si_{11}N_{20}O$ (RE = Yb, Lu; $x \approx 2.2$) were synthesized starting from REF_3, CaH_2, and "$Si(NH)_2$" in a radiofrequency furnace at 1600 or 1400 °C, respectively. The crystal structure was solved and refined from single-crystal X-ray diffraction data of dark red $Yb_{6-x}Ca_{1.5x}Si_{11}N_{20}O$ crystals in the trigonal space group $P31c$ (no. 159) with a = 9.8281(10), c = 10.5968(13) Å and Z = 2. The structure represents a filled variant of the $Er_6Si_{11}N_{20}O$ structure type, in which the charge difference caused by substitution of trivalent Yb^{3+} with bivalent Ca^{2+} is balanced by occupation of an additional third cation site. Synthesis of $Lu_{6-x}Ca_{1.5x}Si_{11}N_{20}O:Ce^{3+}$ resulted in a yellow powder with yellow luminescence. Powder X-ray data were analyzed by Rietveld refinement based on the crystal data obtained from $Yb_{6-x}Ca_{1.5x}Si_{11}N_{20}O$. The Ce^{3+} doped compound exhibits a broad emission (fwhm ≈ 168 nm/≈ 5100 cm^{-1}) with a maximum at $\lambda_{em} \approx 565$ nm. The emission extends more in the red spectral range compared to YAG:Ce^{3+}, thus making it an interesting phosphor for warm-white single phosphor converted light-emitting diodes (1pcLED) with an improved color rendering index.

Introduction

According to the U.S. Department of Energy Solid-State Lighting Program, light-emitting diodes (LEDs) are revolutionizing the lighting market and offer new opportunities in the field of illumination design and energy efficiency. The energy savings of LED white-light sources will reduce the U.S. lighting energy consumption by nearly one-half in 2030 and about 75 % by 2035 compared to conventional white-light sources. LEDs, that had their breakthrough with "*the invention of efficient blue light-emitting diodes which has enabled bright and energy-saving white light sources*"[1] based on (In,Ga)N by Akasaki, Amano and Nakamura, have surpassed many conventional lighting technologies (i.e. incandescent, halogen, fluorescent and high-intensity discharge) in terms of energy efficiency, lifetime and color quality.[1,2] However, ongoing research in the field of phosphor-converted LEDs (pcLEDs) is indispensable to realize the forecasts. Commonly used state-of-the-art white light single phosphor converted light-emitting diodes (1pcLEDs) are based on $Y_{3-x}Gd_xAl_{5-y}Ga_yO_{12}:Ce^{3+}$ (YAG:Ce^{3+}), a broadband, yellow emitting phosphor (λ_{em} = 530–560 nm).[3–6] A drawback of the YAG:Ce^{3+} phosphor is its limitation to cool-white light applications (correlated color temperature CCT = 4000–8000 K, color rendering index CRI < 75) due to the lack of red spectral components. To achieve a natural color perception for illumination-grade lighting applications, higher CRI values are strongly sought-after.[3,7] Improvements can be accomplished by either adding red emitting phosphors such as $Sr_xCa_{1-x}AlSiN_3:Eu^{2+}$, $Ba_2Si_5N_8:Eu^{2+}$ or $Sr[LiAlN_3]:Eu^{2+}$ [8–10] in 2pcLED or by developing new phosphors with a red-shifted emission compared to YAG:Ce^{3+} in a 1pcLED approach. Nitridoaluminates and nitridosilicates with their highly condensed structures have turned out to be promising host materials with excellent thermal and chemical stability. Their predominantly covalent activator–nitrogen bonds shift the photoluminescence emission into the red spectral range (nephelauxetic effect), which leads to lower, i.e. warmer color temperatures as it is requested for warm-white LEDs.[11–13] This makes Ce^{3+}-doped nitridosilicates to highly promising phosphors for application in warm-white 1pcLEDs. Examples for such recently developed phosphors are $(La,Ca)_3Si_6N_{11}:Ce^{3+}$, $La_3BaSi_5N_9O_2:Ce^{3+}$, $CaAlSiN_3:Ce^{3+}$ and $SrAlSi_4N_7:Ce^{3+}$.[14–17] In general, Ce^{3+} phosphors are more suited than Eu^{2+} phosphors for applications where high luminance is important.[18] New Ce^{3+} phosphors are especially needed for high intensity light sources with superior color rendering quality. In this contribution, we report on the synthesis of $Yb_{6-x}Ca_{1.5x}Si_{11}N_{20}O$ and $Lu_{6-x}Ca_{1.5x}Si_{11}N_{20}O$ ($x \approx 2.2$). $Lu_{6-x}Ca_{1.5x}Si_{11}N_{20}O:Ce^{3+}$ shows an interesting luminescence spectrum compared to YAG:Ce^{3+}, which makes it a potential new phos-

[a] *Department of Chemistry, University of Munich (LMU), Butenandstraße 5-13, 81377 Munich, Germany*
E-mail: wolfgang.schnick@uni-muenchen.de
http://www.cup.lmu.de/ac/schnick/
[b] *Lumileds Germany GmbH, Lumileds Phosphor Center Aachen, Philipsstraße 8, 52068 Aachen, Germany*
Supporting information and ORCID(s) from the author(s) for this article are available on the WWW under https://doi.org/10.1002/ejic.201901206.

phor for warm-white 1pcLEDs for illumination-grade lighting applications.

Results and Discussion

Synthesis and Chemical Analysis

The synthesis described in the Experimental Section led to CaF_2 as a side product, which can be easily removed by washing with conc. HNO_3, conc. HCl, H_2O and ethanol. Due to the formation of CaF_2, an excess of CaH_2 had to be used. Dark red crystals (Figure S1) with a size up to 200 µm were obtained. EDX data (Table S1) showed that Ca is present in all investigated crystals. The averaged determined atomic ratios (Yb/Ca/Si/N/O = 11:7:28:51:4) agree well within the limits of accuracy with the theoretical values calculated from the sum formula obtained by single-crystal X-ray diffraction data (Yb/Ca/Si/N/O = 10:8:28:51:3). However, the obtained atomic ratios of Yb and Ca slightly differ in each single measurement, which indicates that the Yb/Ca ratio is moderately variable. This leads to the assumption that the sum formula can be best described with the variable *x*, leading to $Yb_{6-x}Ca_{1.5x}Si_{11}N_{20}O$ ($x \approx 2.2$) as a more accurate description of the entire sample stoichiometry. For determination of the composition of the whole sample, PXRD data were refined with the Rietveld method based on single-crystal X-ray diffraction data. The refinement shows that the synthesis led to phase pure $Yb_{6-x}Ca_{1.5x}Si_{11}N_{20}O$ ($x \approx 2.2$, Figure 1, Table S2).

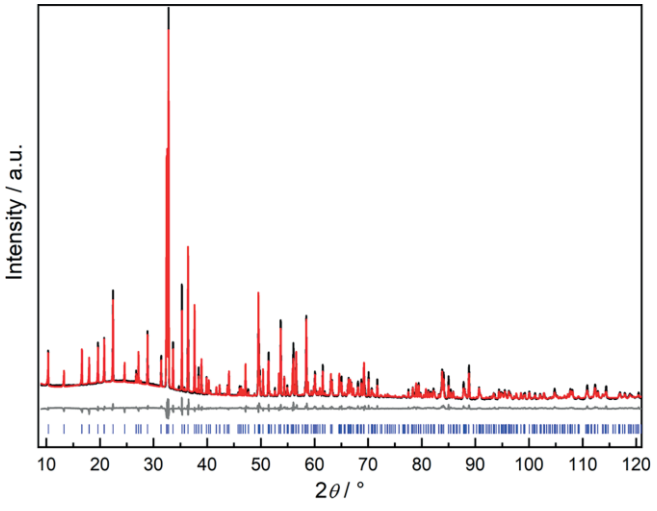

Figure 1. Rietveld refinement of PXRD data collected from an $Yb_{6-x}Ca_{1.5x}Si_{11}N_{20}O$ ($x \approx 2.2$) powder sample with experimental data (black line, Cu-$K_{\alpha 1}$ radiation, λ = 1.54056 Å), calculated pattern (red line), difference profile (gray line) and positions of Bragg reflections (blue bars).

Minor differences in the reflection intensities may be due to slightly variable Yb/Ca ratios on the three cation sites with mixed occupancy. Absence of N–H vibration bands in the FTIR spectrum (Figure S2) show that there are no N–H groups. Synthesis of $Lu_{6-x}Ca_{1.5x}Si_{11}N_{20}O:Eu^{2+}$ led to a pinkish powder with orange-red luminescence under irradiation with blue light, whereas Ce^{3+} doping resulted in a yellow powder with yellow luminescence. The morphology of the sample shows small crystallites with a size up to 10 µm (Figure S3). The averaged values obtained from EDX measurements (Table S3) of a non-doped sample (Lu/Ca/Si/N/O/F = 8:7:26:51:7:1) are comparable to the values measured on $Yb_{6-x}Ca_{1.5x}Si_{11}N_{20}O$ ($x \approx 2.2$) indicating that the previously obtained sum formula is also applicable. The O value is slightly increased presumably due to superficially bound O. Despite washing of the samples a small residue of CaF_2 is still left which can be analyzed by detection of fluorine. The synthesis of $Lu_{6-x}Ca_{1.5x}Si_{11}N_{20}O$ did not yield single crystals. Therefore, the single-crystal X-ray diffraction data of $Yb_{6-x}Ca_{1.5x}Si_{11}N_{20}O$ ($x \approx 2.2$) were modified and applied for Rietveld refinement of a washed, non-doped sample, which shows no CaF_2 side phase although minor amounts of fluorine were detected by EDX measurements (Figure 2, Table S4).

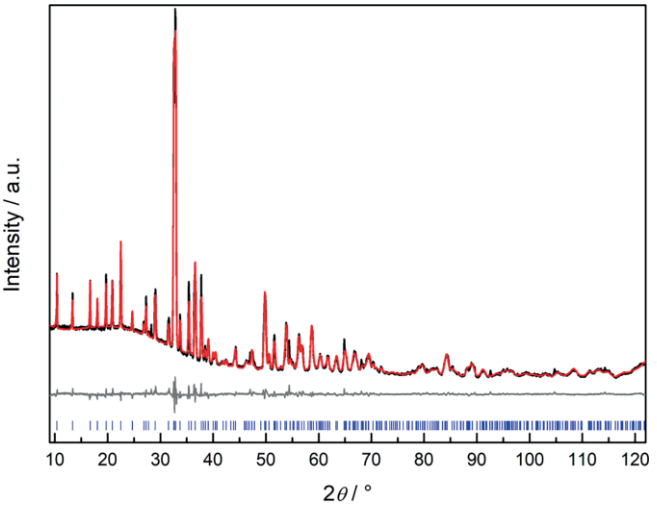

Figure 2. Rietveld refinement of PXRD data collected from a $Lu_{6-x}Ca_{1.5x}Si_{11}N_{20}O$ sample with experimental data (black line, Cu-$K_{\alpha 1}$ radiation, λ = 1.54056 Å), calculated pattern (red line), difference profile (gray line) and positions of Bragg reflections (blue bars).

Due to the good accordance of the Rietveld and EDX data compared to $Yb_{6-x}Ca_{1.5x}Si_{11}N_{20}O$ ($x \approx 2.2$), the sum formula $Lu_{6-x}Ca_{1.5x}Si_{11}N_{20}O$ with the same crystal structure can be assumed. Reflection intensity differences are again caused by small differences in the Lu/Ca ratio distributed over the entire sample.

Crystal Structure Determination

The crystal structure of $Yb_{6-x}Ca_{1.5x}Si_{11}N_{20}O$ ($x \approx 2.2$) was solved and refined from single-crystal X-ray diffraction data in the trigonal space group *P*31*c* (no. 159), in which all atoms were refined with anisotropic displacement parameters. The crystallographic data of the refinement are summarized in Table 1. Atomic coordinates, isotropic displacement parameters, site occupancy factors (Table S5) as well as the anisotropic displacement parameters (Table S6) are summarized in the Supporting Information. $Yb_{6-x}Ca_{1.5x}Si_{11}N_{20}O$ ($x \approx 2.2$) crystallizes in a filled variant of the $Er_6Si_{11}N_{20}O$ structure type, first described by *Woike* et al. and subsequently with minor differences regarding the occupation of cation sites reported by *Köllisch* et al.[20,21] The structure exhibits a three-dimensional network of vertex sharing SiN_4 tetrahedra (Figure 3), which contains terminal

[N[1]], twofold [N[2]], threefold [N[3]] and even fourfold [N[4]] bridging nitrogen atoms.[20–26,13] The terminal nitrogen atom in $Er_6Si_{11}N_{20}O$ was a novel feature in nitridosilicates.[20] The most unusual feature of the structure is the simultaneous occurrence of all functionalities N[1] to N[4].[21]

Condensation of six SiN_4 tetrahedra leads to the formation of *sechser* rings (Figure 4a), which are linked by SiN_4 tetrahedra to sheets perpendicular to [001].[27]

Table 1. Crystallographic data of the single-crystal structure determination of $Yb_{6-x}Ca_{1.5x}Si_{11}N_{20}O$ (x ≈ 2.2).

Formula	$Yb_{3.79}Ca_{3.22}Si_{11}N_{20}O$
formula mass [g mol^{-1}]	1389.00
crystal system	trigonal
space group	*P*31*c* (no. 159)
lattice parameters [Å]	*a* = 9.8281(10)
	c = 10.5968(13)
cell volume [Å^3]	886.4(2)
formula units/unit cell	2
X-ray density [g cm^{-3}]	5.208
abs. coefficient [μ mm^{-1}]	21.515
absorption correction	Multiscan[19]
temperature [K]	293(2)
diffractometer	Bruker D8 Venture
radiation [Å]	Mo-K_α (λ = 0.71073)
F(000)	1264
θ range [°]	3.8297 ≤ θ ≤ 32.2982
independent reflections	1776
refined parameters/restraints	128/7
GoF	1.030
R_{int}	0.0962
R_σ	0.0443
*R*1 (all data/for $I > 2\sigma(I)$)	0.0428/0.0418
*wR*2 (all data/for $I > 2\sigma(I)$)	0.1008/0.1002
$\Delta\rho_{max}/\Delta\rho_{min}$ (e Å^{-3})	1.881/–2.386

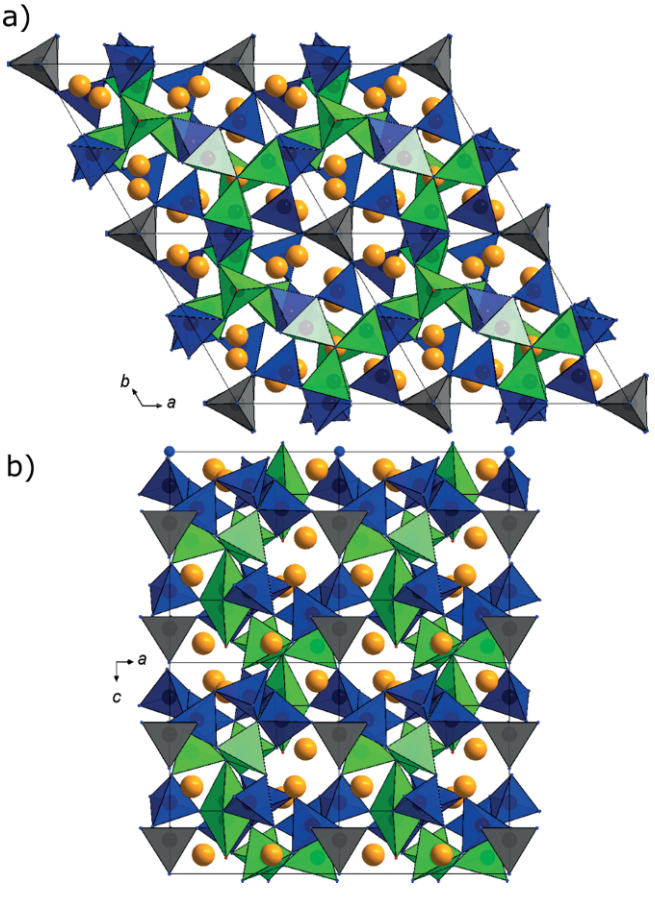

Figure 3. Crystal structure of an $Yb_{6-x}Ca_{1.5x}Si_{11}N_{20}O$ (*x* ≈ 2.2) 2×2×2 super cell viewed along (a) [001] and (b) [010]. SiN_4 tetrahedra in blue, green and gray, N atoms blue and Yb/Ca atoms orange. Unit cell in black.

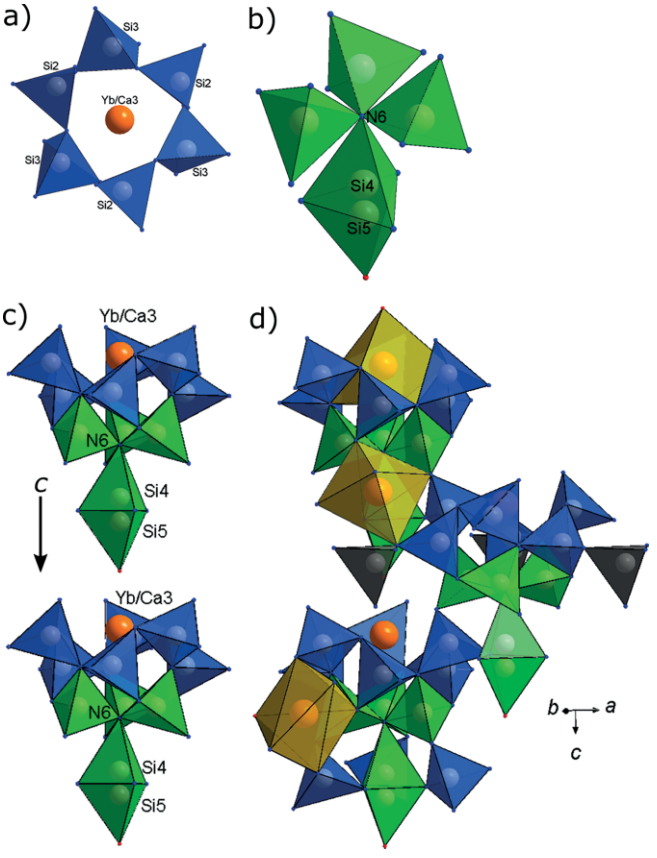

Figure 4. (a) *Sechser* rings of SiN_4 tetrahedra (blue) with centered Yb/Ca3 site. (b) Star shaped unit (green SiN_4 tetrahedra) containing the fourfold bridging N6 atom and the Si4/Si5 split position. (c) Combinations of ring and star shaped units stacked along [001]. (d) Linkage of units in different [001] columns by common corners and via additional tetrahedra (gray) containing the terminal N7 atom. N atoms blue, O atoms red and Yb/Ca atoms orange.

The connecting tetrahedra contain the terminal nitrogen atoms (N7, gray tetrahedra) aligned in the [001] direction. The rings are connected to a star shaped unit containing the fourfold bridging nitrogen atom (N6[4], green tetrahedra, Figure 4b). This unit contains also a Si4/Si5 split position (52 %/48 %) with Si5 in a SiN_3O[1] tetrahedron. In contrast to *Woike* et al. and *Köllisch* et al., the oxygen site was not refined with a split position but with an enlarged anisotropic displacement parameter along [001], which is oriented in the direction of the columns formed by the sechser rings and the star shaped unit. Difference Fourier syntheses ($F_{obs} - F_{calc}$) of the electron density located at the O1[1] site as well as at the N6[4] site, which has also an enlarged anisotropic displacement parameter, do also not indicate a splitting of the electron density at high isosurface levels unlike the Si4/Si5 split position (Figure S4). The enlarged anisotropic displacement parameters may be caused by the Si4/Si5 split position. The units combined via common SiN_4

tetrahedra corners of the ring and star shaped unit with the split position are stacked along the [001] direction (Figure 4c). The different so formed columns are shifted against each other in [001] and linked via the star shaped unit of one column to the ring of another column and vice versa (Figure 4d).

There are three different cation sites with mixed occupancy of Yb and Ca (Figure 5). Yb/Ca1 (76 %/24 %) is coordinated by six nitrogen atoms in a distorted octahedron and Yb/Ca2 (47 %/53 %) coordinated by five nitrogen and one oxygen atoms forms a distorted trigonal prism. The three cation sites are linked by common edges (Yb/Ca1 to Yb/Ca2 and Yb/Ca2 to Yb/Ca3) or corners (Yb/Ca1 to Yb/Ca3). In contrast to the $Er_6Si_{11}N_{20}O$ structure type,[20] which exhibits only two cation sites, a third cation site is occupied in $Yb_{6-x}Ca_{1.5x}Si_{11}N_{20}O$ ($x \approx 2.2$) by 9 % Yb and 91 % Ca in a sevenfold coordination of six nitrogen (N4: 2.547(12) Å, N8: 2.564(10) Å) and one oxygen atom (2.27(3) Å). It can be described by three N4 and three N8 each in a plane twisted against each other forming a zigzag pattern. The coordination sphere is completed by the terminal oxygen atom of the SiN_3O tetrahedra, which coordinates Si5 of the Si4/Si5 split position of the star shaped unit connected to the *sechser* ring stacked along [001]. This structural situation but with an under-occupied third cation site located inside the *sechser* rings was also reported by *Köllisch* et al. in contrast to the published structure type.[20,21] Due to very similar atomic form factors of O^{2-} and N^{3-}, an unequivocal assignment of O and N only by means of X-ray methods is not possible. The explanation of *Woike* et al. for the presence and location of oxygen is only based on structure-chemical arguments like charge balance and its proximity to a potential third cation site occupied by one third in a possible "$Er_{6.33}Si_{11}N_{21}$" structure (Er3–N: 2.37(3) Å), in which oxygen is replaced by nitrogen for charge balance. The oxygen site is split due to the Si4a/Si4b split position and is nearly trigonal planar coordinated by three Er atoms.[20] In contrast, *Köllisch* et al. argue that the occupation of the third cation site is necessary to form a tetrahedral coordination of Er for the oxygen atom. Such oxygen centered $[Ln_4O]^{10+}$ ions, which stabilize oxygen atoms that can be considered as not belonging to the silicate anion structure due to the long distance to Si, have already been reported.[21,28–30] In the title compound, the third cation site has to be occupied in order to compensate the charges unbalanced by mixed occupancy of the first two cation sites with divalent and trivalent cations. XRD and EDX data support this assumption. To confirm the assumed anion arrangement, lattice energy (MAPLE)[31–33] and bond valence sum (BVS)[34,35] calculations were performed. For MAPLE calculations of $Yb_{3.79}Ca_{3.22}Si_{11}N_{20}O$ as well as for "$Yb_6Si_{11}N_{20}O$" ($Er_6Si_{11}N_{20}O$ structure type[21] with Er substituted by Yb) some approximations had to be made (Table S7). The partial MAPLE values calculated for Yb/Ca1–3 are in good agreement with typical MAPLE values for RE^{3+} and Ca^{2+} in nitridosilicates and with the values calculated for "$Yb_6Si_{11}N_{20}O$".[13] The Si values are also in good accordance despite the Si split position. Only the value of Si6 is slightly enlarged even compared to "$Yb_6Si_{11}N_{20}O$".[13] The values of the anions are again in good agreement. The $(Si6)N_4$ tetrahedron contains the terminal nitrogen atom. This site could also be occupied by oxygen, which would explain the high value of Si6 when coordinated only by nitrogen. Substitution of N7 by oxygen ("O7") leads to more reasonable values, but then more Ca has to be incorporated in the structure for charge balance. However, due to the variable mixed occupancy of the cation sites, it is not possible to determine whether the Ca content is caused by an increased oxygen incorporation. Thus, it cannot be clearly stated that Si6 is only coordinated by nitrogen. Another possibility for charge balance is the incorporation of nitrogen on the former O1 site, which is also terminal ("N11"), but the obtained value is too low for known terminal nitrogen atoms. To further differentiate the occupation of the sites by oxygen and nitrogen, BVS calculations were performed (Table S8). The bond valence sums for N1–N6 as well as for N8 are in good agreement with the assignment of nitrogen. The value of the terminal nitrogen N7 is slightly too low for a nitrogen atom, therefore, as in the MAPLE calculations, N7 was replaced by oxygen ("O7"), whose value deviates slightly from the expected –2, but it is closer to that of oxygen than the previous value for nitrogen. The substitution affects the BVS values for Yb/Ca1–3 and Si6, which are still reasonable. As explained for the MAPLE calculation, O1 was substituted by nitrogen ("N11") for charge balance. The obtained value is in the range of the values expected for N and O, respectively, which indicates that both are suitable. MAPLE and BVS calculations agree well with each other, both suggest that oxygen would be more suitable on the N7 site. Incorporation of nitrogen on the former O1 site for charge balance does not solve this problem, so charges could be balanced by Ca. However, the obtained data are insufficient for an unequivocal statement. Since only the boundary conditions were considered, a mixed O/N occupancy is also conceivable. According to Pauling's second rule,[36] O should substitute N near the cation site with the higher Ca content to compensate the locally imbalanced char-

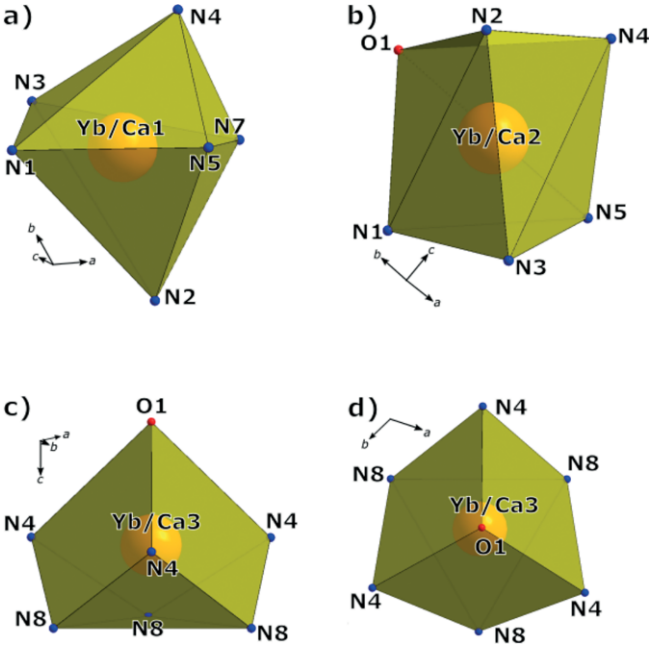

Figure 5. Coordination polyhedra of the three cation sites with mixed Yb/Ca occupancy. (a) Yb/Ca1, (b) Yb/Ca2, (c) Yb/Ca3 side view, (d) Yb/Ca3 top view.

ges caused by substitution of Yb^{3+} by Ca^{2+} in a nitrogenous surrounding. It can be assumed that Yb-N pairs are substituted by Ca-O pairs, which are both charge-neutral.[37] The distribution of Yb and Ca on the different sites seems to depend on the average distances of Yb/Ca to N/O. For Yb/Ca1, the average Yb/Ca1–N distance is about 2.4 Å, Yb/Ca2–N/O about 2.45 Å and Yb/Ca3–N/O about 2.5 Å. The occupation of the sites is in good agreement with the ionic radii, in which the larger Ca^{2+} occupies preferentially the site with the larger distances.[31] During the refinement, sum formula constraints were applied in order to achieve charge neutrality by mixed Yb/Ca occupation of the different cation sites. This leads to a sum formula with a slight excess of negative charges, which, however, coincides within the error limits with a charge neutral sum formula. The Si–N distances (1.691(10)–1.790(7) Å) are in good agreement with the values reported for $Er_6Si_{11}N_{20}O$.[20,21] The Si5–O1 bond length of 1.92(3) Å is slightly enlarged due to the Si4/Si5 split position. The value is in between the values given in the literature for distances to an oxygen split position. According to *Köllisch* et al., this represents a transition state between an isolated oxygen atom (i.e. occupancy of Si4) in a $[Ln_4O]^{10+}$ complex and a terminal oxygen atom in a $(Si5)N_3O^{[1]}$ tetrahedron.[20,21] The Si4–Si5 distance of the split position is 0.929(17) Å, which is slightly larger than reported, because the absence of an oxygen split position allows the Si atoms to further separate. The Yb/Ca–N distances are in the range of 2.340(9)–2.564(10) Å with slightly shorter Yb/Ca2–O1 and Yb/Ca3–O1 bond length of 2.284(2) and 2.27(3) Å, respectively, which are in also good agreement with the reported values.[20,21]

Since no single crystals of $Lu_{6-x}Ca_{1.5x}Si_{11}N_{20}O$ ($x \approx 2.2$) were obtained, no independent structural model was elucidated. However, due to similar EDX results and the accordance of the powder diffraction pattern with the $Yb_{6-x}Ca_{1.5x}Si_{11}N_{20}O$ ($x \approx 2.2$) single-crystal data in the Rietveld refinement, it can be assumed that $Lu_{6-x}Ca_{1.5x}Si_{11}N_{20}O$ ($x \approx 2.2$) is isotypic to $Yb_{6-x}Ca_{1.5x}Si_{11}N_{20}O$. As a result of the potential variable occupation of the cation sites, the Lu/Ca ratio may vary.

UV/Vis Spectroscopy

With respect to the red color of the crystals of $Yb_{6-x}Ca_{1.5x}Si_{11}N_{20}O$ ($x \approx 2.2$), a solid-state UV/Vis spectrum was recorded to determine the optical band gap. The measured diffuse reflectance spectrum of a powder sample was converted into a pseudo-absorption spectrum using the Kubelka–Munk function $F(R) = (1 - R)^2/2R$ with R being the reflectance.[38] Subsequently, the optical band gap was determined from a Tauc plot, where $h\nu$ is plotted against $(F(R)\cdot h\nu)^{1/n}$ with $n = 1/2$ for a direct allowed transition, by drawing a line tangent at the inflection point.[39] The optical band gap was estimated to be approximately 1.87 eV (Figure 6).

The determined optical band gap matches very well with the optical perception of the red crystals. The comparable small band gap of $Yb_{6-x}Ca_{1.5x}Si_{11}N_{20}O$ ($x \approx 2.2$) may be caused by the onset of the valence band-Yb^{3+} charge-transfer band, which is referred to the transition to the localized $4f^{14}$ ground state of Yb^{2+}.[40] Due to the low energetic difference, it can be assumed

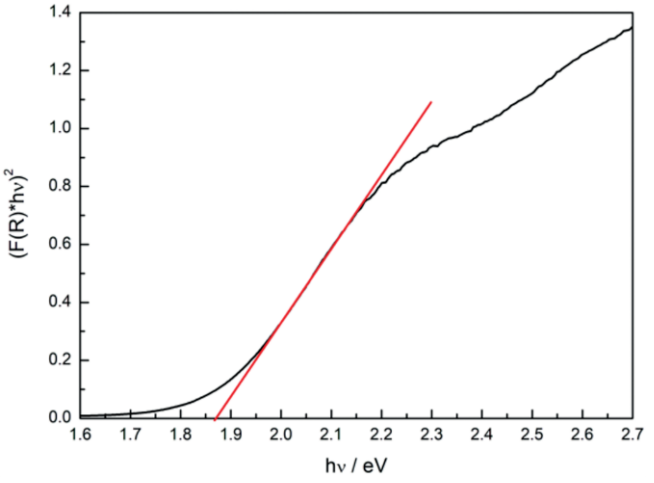

Figure 6. Tauc plot ($n = 1/2$) for an $Yb_{6-x}Ca_{1.5x}Si_{11}N_{20}O$ ($x \approx 2.2$) powder sample.

that the direct transition will be more likely in the visible range. The small band gap of $Yb_{6-x}Ca_{1.5x}Si_{11}N_{20}O$ ($x \approx 2.2$) may be the reason for the absence of luminescence upon doping with Eu^{2+} or Ce^{3+} because the emitted luminescence will be absorbed by the host material itself. The direct band gap of a non-doped $Lu_{6-x}Ca_{1.5x}Si_{11}N_{20}O$ ($x \approx 2.2$) powder sample is approximately 4.5 eV (Figure 7).The band gap corresponds to the valence band-conduction band onset. Here, the direct transition will again probably be more likely due to the low energy difference. The direct band gap makes $Lu_{6-x}Ca_{1.5x}Si_{11}N_{20}O$ ($x \approx 2.2$) a suitable host material for doping, because for pcLED applications wide band gaps ≥ 4 eV are required.

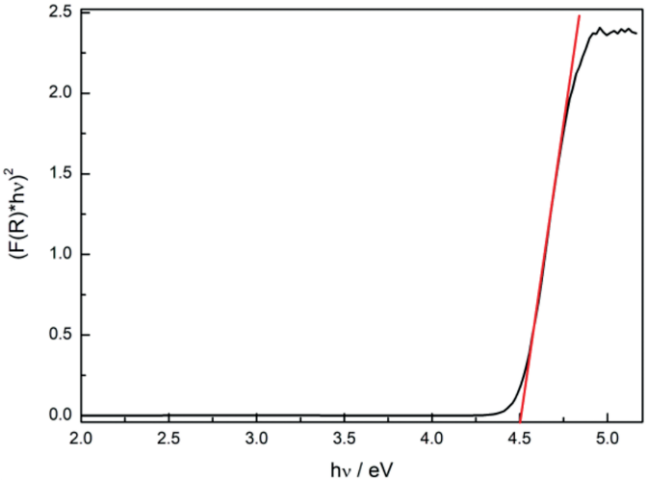

Figure 7. Tauc plot ($n = 1/2$) for a non-doped $Lu_{6-x}Ca_{1.5x}Si_{11}N_{20}O$ ($x \approx 2.2$) powder sample.

Luminescence

Luminescence properties were obtained from thick bed powder samples of $Lu_{6-x}Ca_{1.5x}Si_{11}N_{20}O{:}Eu^{2+}$ and $Lu_{6-x}Ca_{1.5x}Si_{11}N_{20}O{:}Ce^{3+}$ ($x \approx 2.2$). The Eu^{2+} doped compound shows a reddish luminescence upon irradiation with UV to blue light (λ_{exc} = 440 nm) and emits at λ_{em} = 618 nm with a full width at

half-maximum (fwhm) of 124 nm/3000 cm^{-1} (Figure S6). $Lu_{6-x}Ca_{1.5x}Si_{11}N_{20}O:Ce^{3+}$ ($x \approx 2.2$) shows a more interesting luminescence (λ_{exc} = 440 nm, Figure 8).

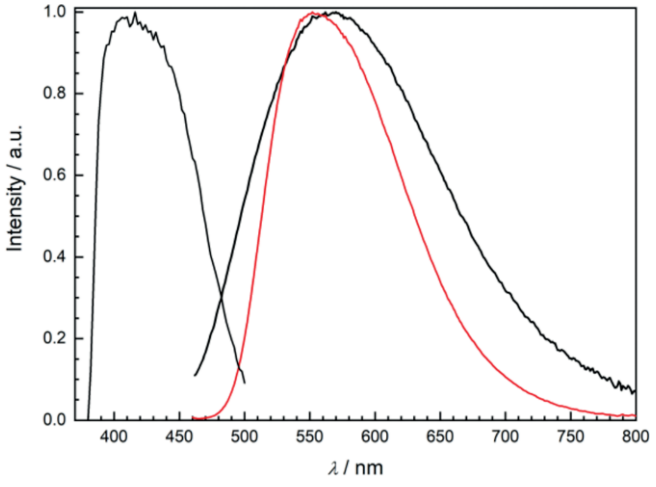

Figure 8. Normalized excitation and emission spectra (λ_{exc} = 440 nm) of $Lu_{6-x}Ca_{1.5x}Si_{11}N_{20}O:Ce^{3+}$ ($x \approx 2.2$, black) compared to YAG:Ce^{3+} (red).

The emission maximum is positioned at λ_{em} = 565 nm with a full width at half-maximum (fwhm) of 168 nm/5100 cm^{-1}, a quantum efficiency of 22 % and color coordinates (CIE 1931, Commission Internationale de l'Éclairage)[41] of x = 0.436 and y = 0.503 (CIE 1960: u = 0.214, v = 0.370). Comparison of the ionic radii indicates that Ce^{3+} (coordination number CN = 6: 1.01 Å, CN = 7: 1.07 Å) preferably replaces Ca^{2+} (CN = 6: 1.00 Å, CN = 7: 1.06 Å) rather than Yb^{3+} (CN = 6: 0.87 Å, CN = 7: 0.93 Å).[31] The broadband emission, which is typical for Ce^{3+}-doped materials, results from a spin and parity allowed transition from the lowest 5d level to the 4f ground state split into the two $^2F_{5/2}$ and $^2F_{7/2}$ levels separated by 2000 cm^{-1}.[42] In addition, occupation of the asymmetric sites Yb/Ca1/2 (Wyckoff positions 6c with site symmetry 1) and Yb/Ca3 (Wyckoff positions 2b with site symmetry 3) with different activator-N/O distances leads to different crystal field interactions and therefore to multiple doublet emissions slightly shifted to each other, resulting in a further broadening. The emission spectrum is compared to an industrially optimized $Y_3Al_5O_{12}:Ce^{3+}$ (YAG:Ce^{3+}, Lumileds Phosphor Center Aachen, Lumileds Germany GmbH), which exhibits an emission maximum at λ_{em} = 552 nm (λ_{exc} = 440 nm) with a full width at half-maximum (fwhm) of 118 nm/3600 cm^{-1} and a quantum efficiency of 95 %. The color coordinates are x = 0.444 and y = 0.537 (u = 0.208, v = 0.377). The $Lu_{6-x}Ca_{1.5x}Si_{11}N_{20}O:Ce^{3+}$ ($x \approx 2.2$) luminescence spectrum shows a comparable emission in the yellow region but with an increased emission in the red spectral range. The color point of $Lu_{6-x}Ca_{1.5x}Si_{11}N_{20}O:Ce^{3+}$, which is assigned in the CIE 1960 color space (Figure 9), is located nearby YAG:Ce^{3+} in the yellow-orange spectral range.

A theoretical white light 1pcLED based on a blue primary LED (λ_{em} = 450 nm) combined with the $Lu_{6-x}Ca_{1.5x}Si_{11}N_{20}O:Ce^{3+}$ phosphor would offer a CCT of about 4800 K (x = 0.352, y = 0.361; u = 0.212, v = 0.327).[43] In comparison, a theoretical

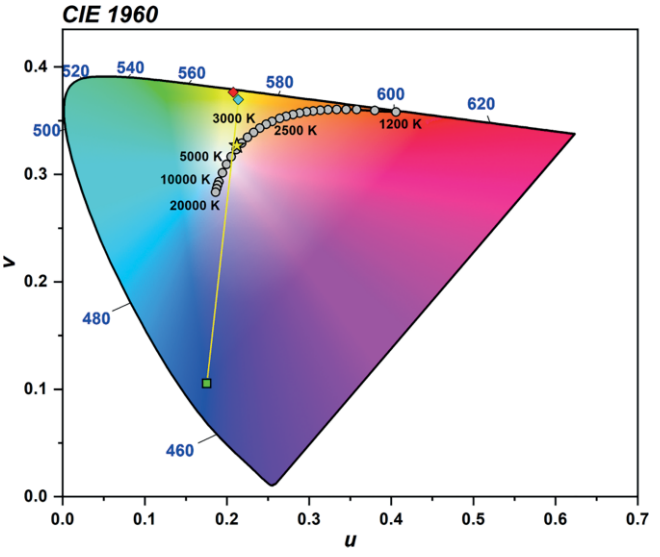

Figure 9. CIE 1960 color space with the color points of $Lu_{6-x}Ca_{1.5x}Si_{11}N_{20}O:Ce^{3+}$ ($x \approx 2.2$; turquoise ◊), YAG:Ce^{3+} (red ◊) and a blue primary LED (green square) along with an ideal blackbody radiator (Planckian locus, black line with gray squares) at different temperatures [K]. Yellow line for determination of the CCT of a theoretical LED based on a blue primary LED and the $Lu_{6-x}Ca_{1.5x}Si_{11}N_{20}O:Ce^{3+}$ phosphor (intersection with Planckian locus indicated with yellow ☆).[41,43]

YAG:Ce^{3+} based 1pcLED exhibits a CCT of approximately 5300 K (x = 0.337, y = 0.350; u = 0.207, v = 0.322). The determined CCT values show that $Lu_{6-x}Ca_{1.5x}Si_{11}N_{20}O:Ce^{3+}$ could offer slightly lower CCT values and could therefore be used in warm-white light applications. However, the main advantage is the increased output in the red spectral range, which could lead to improved CRI compared to a YAG:Ce^{3+} based LED. As a main benefit of the title compound, color rendition R_a increases significantly from 68 to 84 (R_9 = 29), a typical value of illumination grade white LEDs. This could make $Lu_{6-x}Ca_{1.5x}Si_{11}N_{20}O:Ce^{3+}$ a potentially better phosphor for applications with a higher color rendering index in warm-white 1pcLED than YAG:Ce^{3+}, which leads only to cool, pale white light in combination with a blue emitting (In,Ga)N primary LED.

Another yellow phosphor, $Y_{6+(x/3)-y}Ca_{y+(z/2)}Si_{11}N_{20+x-y+z}O_{1-x+y-z}$:Ce, which crystallizes analogously to $Lu_{6-x}Ca_{1.5x}Si_{11}N_{20}O$ in the same crystal structure reported by *Woike* et al. with three mixed occupied cation sites, exhibits an emission maximum at λ_{em} = 554 nm (λ_{exc} = 450 nm) with fwhm of 147 nm. This phosphor was claimed to be used in general white lighting devices requiring high color rendering due to its broad yellow emission.[44] In comparison to YAG:Ce^{3+}, the emission maximum of $Y_{6+(x/3)-y}Ca_{y+(z/2)}Si_{11}N_{20+x-y+z}O_{1-x+y-z}$:Ce stays almost unchanged but with a broader emission. However, $Lu_{6-x}Ca_{1.5x}Si_{11}N_{20}O:Ce^{3+}$ exhibits a slightly red-shifted emission maximum with an even broader fwhm extending in the red spectral range. So it is expected that $Lu_{6-x}Ca_{1.5x}Si_{11}N_{20}O:Ce^{3+}$ offers an even better color rendering than $Y_{6+(x/3)-y}Ca_{y+(z/2)}Si_{11}N_{20+x-y+z}O_{1-x+y-z}$:Ce due to its increased red spectral output.

The quantum efficiency of $Lu_{6-x}Ca_{1.5x}Si_{11}N_{20}O:Ce^{3+}$ with 22 % at room temperature is rather low compared to the industrially optimized YAG:Ce^{3+}. Based on the quantum efficiency of

22 % at room temperature, the quantum efficiency at 6 K can be estimated to about 80 % (Figure 10).

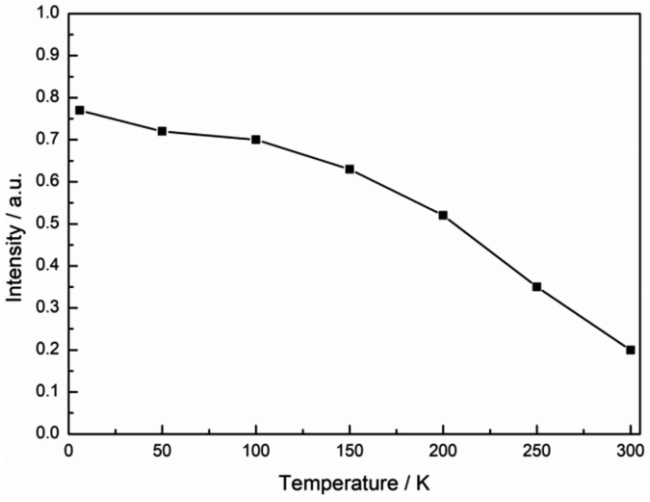

Figure 10. Temperature dependent internal quantum efficiencies of $Lu_{6-x}Ca_{1.5x}Si_{11}N_{20}O:Ce^{3+}$ ($x \approx 2.2$).

From thermal quenching investigations could be expected that the internal quantum efficiency can be increased by about 20 % by lowering the excited $4f^05d^1$ state of Ce^{3+} energetically relative to the bottom of the conduction band. Practically, this may be achieved by partial replacement of Ca^{2+} by heavier alkaline earth elements as being discussed in literature.[45]

The influence of the dopant concentrations are investigated by comparison of samples with a nominal dopant content of 0.5, 1, 2 and 4 Mol-% Ce^{3+} referred to Ca (Figure 11, Table S9).

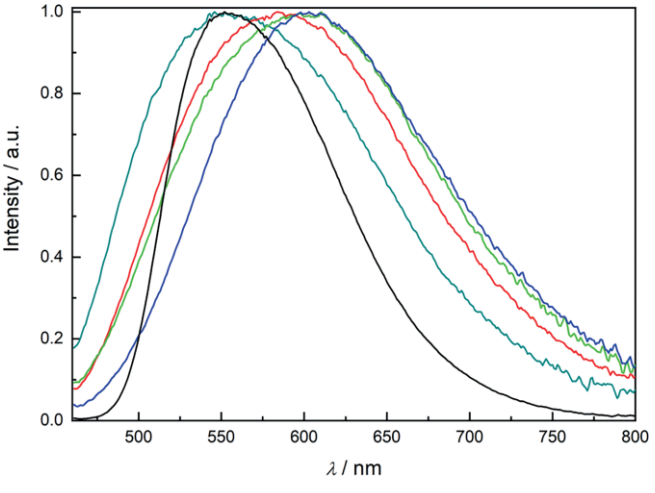

Figure 11. Normalized emission spectra (λ_{exc} = 440 nm) of $Lu_{6-x}Ca_{1.5x}Si_{11}N_{20}O:Ce^{3+}$ ($x \approx 2.2$) with different dopant concentrations of 0.5 % (turquoise line), 1 % (red line), 2 % (green line) and 4 % (blue line) compared to YAG:Ce (black line).

Increasing the dopant concentration leads to a red-shifted emission while fwhm remains largely constant. Phosphors having multiple emission sites can exhibit rather large emission maxima shifts at different doping concentrations because the occupancy of the available activator sites can change significantly depending on the doping concentration and synthesis conditions. Even the quantum efficiency shows no significant or systematic changes and therefore no concentration quenching at the investigated dopant contents (Table S9). There is also no systematic change of the lattice parameters despite increasing the dopant concentration and therefore incorporating a slightly lager cation.

Conclusions

$Yb_{6-x}Ca_{1.5x}Si_{11}N_{20}O$ and $Lu_{6-x}Ca_{1.5x}Si_{11}N_{20}O$ ($x \approx 2.2$) were synthesized in a solid-state reaction and crystallize in a filled variant of the $Er_6Si_{11}N_{20}O$ structure type. The refinement of the $Yb_{6-x}Ca_{1.5x}Si_{11}N_{20}O$ ($x \approx 2.2$) single-crystal X-ray diffraction data shows that Ca is incorporated by mixed occupancy of the two cation sites known from the $Er_6Si_{11}N_{20}O$ structure type as well as an additional third cation site for charge balance. The results are confirmed by EDX measurements, Rietveld refinements and both MAPLE and BVS calculations. The replacement of Yb/Lu by Ca leads to new structural features and could lead to the incorporation of oxygen in the anionic framework, which could have an influence on the luminescence properties. Furthermore, the third cation site is in contrast to the $Er_6Si_{11}N_{20}O$ structure type reported by *Woike* et al. only occupied if Ca is present. Ce^{3+} presumably occupies the Ca^{2+} sites due to similar radii, therefore the sites preferably occupied by Ce could be identified. However, it was not possible to unequivocally distinguish O and N, therefore, neutron diffraction would be necessary as a subject of further research. Rietveld refinement of $Lu_{6-x}Ca_{1.5x}Si_{11}N_{20}O$ ($x \approx 2.2$) was based on the refined single-crystal X-ray diffraction data of $Yb_{6-x}Ca_{1.5x}Si_{11}N_{20}O$ ($x \approx 2.2$), which indicates that both compounds crystallize in the same structure type. The Eu^{2+} doped compound emits at λ_{em} = 618 nm with a full width at half-maximum (fwhm) of 124 nm/3000 cm^{-1}. $Lu_{6-x}Ca_{1.5x}Si_{11}N_{20}O:Ce^{3+}$ ($x \approx 2.2$) exhibits a more interesting luminescence in the yellow spectral range. With λ_{em} = 565 nm and fwhm of 168 nm/5100 cm^{-1}, the phosphor shows a comparable emission to $Y_3Al_5O_{12}:Ce^{3+}$, which is used in 1pcLED but is limited in application due to its cold-white light upon excitation with a (In,Ga)N primary LED. $Lu_{6-x}Ca_{1.5x}>Si_{11}N_{20}O:Ce^{3+}$ ($x \approx 2.2$) emits further in the red spectral region, leading to warm-white light, which offers warmer color temperatures and a higher color rendering index and could therefore be more suited for illumination-grade lighting applications. An (In,Ga)N based LED exhibit an excitation wavelength of 435 nm, which makes $Lu_{6-x}Ca_{1.5x}Si_{11}N_{20}O:Ce^{3+}$ ($x \approx 2.2$) suitable for application in LEDs. Further research is necessary to optimize the quantum efficiency and therefore make $Lu_{6-x}Ca_{1.5x}Si_{11}N_{20}O:Ce^{3+}$ ($x \approx 2.2$) an even more interesting phosphor for modern illumination-grade warm-white lighting applications with increased color rendering index.

Experimental Section

Synthesis: All synthesis steps were performed in an argon-filled glovebox (Unilab, MBraun, Garching; O_2 < 1 ppm; H_2O < 1 ppm). For synthesis of $Yb_{6-x}Ca_{1.5x}Si_{11}N_{20}O$, YbF_3 (0.7055 mmol, 162.3 mg; Alfa Aesar, 99.99 %), Yb_2O_3 (0.0705 mmol, 27.8 mg; smart elements,

99.99 %), CaH_2 (1.6932 mmol, 71.3 mg; Sigma-Aldrich, 99.99 %) and Si_3N_4 (0.7760 mmol, 108.9 mg; Ube Industries, SN-E10) were thoroughly ground in an agate mortar and filled into a tungsten crucible, which was then transferred into a water-cooled silica glass reactor of a radiofrequency furnace (type TIG 10/100; Hüttinger Elektronik Freiburg) attached to a Schlenk line. Under purified N_2-atmosphere, the crucible was heated to 1600 °C in 10 min. The temperature was maintained for 5 h, cooled to 900 °C in 3 h and finally quenched to room temperature. Dark red crystals were obtained, which are stable towards air, water and concentrated mineral acids in repeated washing steps. $Lu_{6-x}Ca_{1.5x}Si_{11}N_{20}O$ was synthesized starting from LuF_3 (0.7017 mmol, 197.4 mg; Sigma-Aldrich, 99.99 %), Lu_2O_3 (0.0702 mmol, 27.9 mg; ABCR, 99.9 %), CaH_2 (1.6840 mmol, 70.9 mg; Sigma-Aldrich, 99.99 %), Si_3N_4 (0.7718 mmol, 108.3 mg; Ube Industries, SN-E10) and with Eu_2O_3 (ABCR, 99.99 %) or CeF_3 (Sigma-Aldrich, 99.99 %) as dopants. The thoroughly ground starting materials were filled into a tungsten crucible and heated analogously to the Yb compound to a final synthesis temperature of 1400 °C. Eu^{2+} doping yielded a pinkish powder with orange-red luminescence under irradiation with blue light, whereas Ce^{3+} doping resulted in a yellow powder with yellow luminescence. The products are stable towards air, water and concentrated mineral acids in repeated washing steps.

Electron Microscopy: For investigation of the chemical composition and morphology of all samples, a scanning electron microscope (SEM) NanoLab G3 (Helios) equipped with an X-Max 80 SDD detector (Oxford Instruments) for energy dispersive X-ray (EDX) measurements was used. The measurements were performed with an acceleration voltage of 20 kV. A carbon-coating (BAL-TEC MED 020, Bal Tec AG) was applied to prevent electrostatic charging of the samples.

Single-Crystal X-ray Diffraction: A single crystal of $Yb_{6-x}Ca_{1.5x}Si_{11}N_{20}O$ ($x \approx 2.2$) was isolated and fixed on a MicroMount (MiTeGen) with an aperture size of 200 µm. X-ray diffraction data were collected with a Bruker D8 Venture diffractometer with rotating anode (Mo-K_α radiation). SADABS was used for absorption correction.[19] The crystal structure was solved using Direct Methods (SHELXS-97) and refined by least-squares methods (SHELXL-97).[46–48]

Further details of the crystal structure investigation(s) may be obtained from Fachinformationszentrum Karlsruhe, 76344 Eggenstein-Leopoldshafen, Germany (fax: +49-7247-808-666; e-mail: crysdata@fiz-karlsruhe.de), on quoting the deposition number CSD-1948717.

Powder X-ray Diffraction: For powder X-ray diffraction (PXRD), the ground samples were sealed into glass capillaries (0.1 mm diameter, wall thickness 0.01 mm; Hilgenberg GmbH, Malsfeld, Germany) and measured on a STOE STADI P diffractometer (Cu-$K_{\alpha 1}$ radiation, $\lambda = 1.5406$ Å, Ge(111) monochromator, Mythen1K detector) in parafocusing Debye–Scherrer geometry. The data were Rietveld refined with the TOPAS Academic V6 package applying the fundamental parameters approach (direct convolution of source emission profiles, axial instrument contributions, crystallite size and microstrain effects).[49–52] Absorption effects were corrected using the calculated absorption coefficient. Preferred orientation of crystallites was handled with the spherical harmonics model of fourth order. The structure model of $Yb_{6-x}Ca_{1.5x}Si_{11}N_{20}O$ ($x \approx 2.2$), which was obtained from single-crystal X-ray diffraction data, was used as a starting point for all refinements.

Fourier Transform Infrared (FTIR) Spectroscopy: An FTIR spectrum of $Yb_{6-x}Ca_{1.5x}Si_{11}N_{20}O$ ($x \approx 2.2$) was measured with a Jasco FT/IR-4100 spectrometer using the ATR method.

UV/Vis Spectroscopy: For the measurement of diffuse reflectance spectra of $RE_{6-x}Ca_{1.5x}Si_{11}N_{20}O$ (*RE* = Yb, Lu; $x \approx 2.2$) in the range of 240 to 800 nm with 1 nm step size, a Jasco V-650 UV/Vis spectrophotometer equipped with a deuterium and a halogen lamp (Czerny-Turner monochromator with 1200 lines/mm concave grating, photomultiplier tube detector) was used.

Luminescence: Photoluminescence properties of $Lu_{6-x}Ca_{1.5x}Si_{11}N_{20}O$:*RE* (*RE* = Eu^{2+}, Ce^{3+}; $x \approx 2.2$) were measured on microcrystalline powder samples in PTFE sample holders using an in-house built system (5.3 in. integrating sphere, spectrofluorimeter equipped with a 150 W Xe lamp, two 500 mm Czerny-Turner monochromators, 1800 1/mm lattices, 250/500 nm lamps with a spectral range from 230 to 820 nm). Determination of the internal quantum efficiency (IQE) was accomplished by comparing integrated emission intensities and absorption at excitation wavelength with standard materials ($BaSO_4$, Merck p.a.; commercial (Sr,Ca)$AlSiN_3$:Eu^{2+}, Mitsubishi Chemical, and $Y_3Al_5O_{12}$:Ce^{3+}, Philips). For investigations on thermal quenching of the emission, an AvaSpec-2048 spectrometer and a stabilized light-emitting-diode (LED) light source was used for sample excitation. Cryospectroscopy between 300 and 6 K was measured on a thick-bed powder layer with a fiber-coupled spectroscopy system containing a thermally stabilized LED light source and a fiber-optic spectrometer (HR2000+ES spectrometer, Ocean Optics) with the sample placed in an evacuated cooling chamber, equipped with a liquid-He compressor system (ARS4HW, Advance Research System Inc.).

Acknowledgments

We thank Dr. Peter Mayer from the Department of Chemistry at University of Munich (LMU) for the collection of the single-crystal data and Petra Huppertz, Detlef Wiechert, Dr. Philipp Strobel, and Volker Weiler (all at Lumileds Phosphor Center Aachen) for luminescence measurements. Inspiring discussions with Dr. Christian Maak (Department of Chemistry, LMU) are gratefully appreciated.

Keywords: Luminescence · High-temperature chemistry · Structure elucidation · Solid-state reactions · Rare earths

[1] *Energy Savings Forecast of Solid-State Lighting in General Illumination Applications*. Building Technologies Office, Energy Efficiency and Renewable Energy, U. S. Department of Energy: Washington, D. C. **2016**.
[2] J. Heber, Nobel Prize **2014**: Akasaki, Amano & Nakamura. *Nat. Phys.* **2014**, *10*, 791.
[3] P. Pust, P. J. Schmidt, W. Schnick, *Nat. Mater.* **2015**, *14*, 454–458.
[4] G. Blasse, A. Bril, *Appl. Phys. Lett.* **1967**, *11*, 53–55.
[5] Z. Xia, A. Meijerink, *Chem. Soc. Rev.* **2017**, *46*, 275–299.
[6] H. A. Höppe, *Angew. Chem. Int. Ed.* **2009**, *48*, 3572–3582; *Angew. Chem.* **2009**, *121*, 3626–3636.
[7] Y. Narukawa, J. Narita, T. Sakamoto, T. Yamada, H. Narimatsu, M. Sano, T. Mukai, *Phys. Status Solidi A* **2007**, *204*, 2087–2093.
[8] H. Watanabe, N. Kijima, *J. Alloys Compd.* **2009**, *475*, 434–439.
[9] H. A. Höppe, H. Lutz, P. Morys, W. Schnick, A. Seilmeier, *J. Phys. Chem. Solids* **2000**, *61*, 2001–2006.
[10] P. Pust, V. Weiler, C. Hecht, A. Tücks, A. S. Wochnik, A.-K. Henß, D. Wiechert, C. Scheu, P. J. Schmidt, W. Schnick, *Nat. Mater.* **2014**, *13*, 891–896.
[11] C. Feldmann, *Z. Anorg. Allg. Chem.* **2012**, *638*, 2169–2171.
[12] S. Schmiechen, P. Pust, P. J. Schmidt, W. Schnick, *Nachr. Chem.* **2014**, *62*, 847–851.
[13] M. Zeuner, S. Pagano, W. Schnick, *Angew. Chem. Int. Ed.* **2011**, *50*, 7754–7775; *Angew. Chem.* **2011**, *123*, 7898–7920.
[14] T. Suehiro, N. Hirosaki, R.-J. Xie, *ACS Appl. Mater. Interfaces* **2011**, *3*, 811–816.
[15] D. Durach, L. Neudert, P. J. Schmidt, O. Oeckler, W. Schnick, *Chem. Mater.* **2015**, *27*, 4832–4838.
[16] Y. Q. Li, N. Hirosaki, R.-J. Xie, T. Takeda, M. Mitomo, *Chem. Mater.* **2008**, *20*, 6704–6714.

[17] J. Ruan, R.-J. Xie, S. Funahashi, Y. Tanaka, T. Takeda, T. Suehiro, N. Hirosaki, Y.-Q. Li, *J. Solid State Chem.* **2013**, *208*, 50–57.
[18] J. Bhardwaj, J. Cesaratto, I. Wildeson, H. Choy, A. Tandon, W. Soer, P. Schmidt, B. Spinger, P. Deb, O. Shchekin, W. Götz, *Phys. Status Solidi A* **2017**, *214*, 1600826.
[19] G. M. Sheldrick, *SADABS, v. 2: Multi-Scan Absorption Correction;* Bruker-AXS: Billerica, MA, **2012**.
[20] M. Woike, W. Jeitschko, *J. Solid State Chem.* **1997**, *129*, 312–319.
[21] K. Köllisch, H. Höppe, H. Huppertz, M. Orth, W. Schnick, *Z. Anorg. Allg. Chem.* **2001**, *627*, 1371–1376.
[22] H. Huppertz, O. Oeckler, A. Lieb, R. Glaum, D. Johrendt, M. Tegel, R. Kaindl, W. Schnick, *Chem. Eur. J.* **2012**, *18*, 10857–10864.
[23] H. Huppertz, W. Schnick, *Angew. Chem. Int. Ed. Engl.* **1996**, *35*, 1983–1984; *Angew. Chem.* **1996**, *108*, 2115–2116.
[24] A. Lieb, J. A. Kechele, R. Kraut, W. Schnick, *Z. Anorg. Allg. Chem.* **2007**, *633*, 166–171.
[25] A. Lieb, W. Schnick, *Solid State Sci.* **2006**, *8*, 185–191.
[26] V. Vinograd, E. Juarez-Arellano, A. Lieb, K. Knorr, W. Schnick, J. D. Gale, B. Winkler, *Z. Kristallogr.* **2007**, *222*, 402–415.
[27] The term *sechser* ring was established by F. Liebau and is derived from the German word "sechser". A *sechser* ring comprises six tetrahedra centers. F. Liebau, *Structural Chemistry of Silicates*, Springer, Berlin, **1985**.
[28] R. Lauterbach, E. Irran, P. Henry, M. Weller, W. Schnick, *J. Mater. Chem.* **2000**, *10*, 1357–1364.
[29] E. Irran, K. Köllisch, S. Leoni, R. Nesper, P. Henry, M. Weller, W. Schnick, *Chem. Eur. J.* **2000**, *6*, 2714–2720.
[30] S. Krivovichev, S. Filatov, T. Semenova, *Russ. Chem. Rev.* **1998**, *67*, 137–155.
[31] R. D. Shannon, *Acta Crystallogr., Sect. AActa Crystallogr., Sect. A: Cryst. Phys. Diffr.,. Theor. Gen. Crystallogr.* **1976**, *32*, 751–767.
[32] R. Hübenthal, *Maple, Program for the Calculation of MAPLE values, version 4*; University of Gießen: Gießen, Germany, **1993**.
[33] R. Hoppe, *Angew. Chem. Int. Ed. Engl.* **1966**, *5*, 95–106; *Angew. Chem.* **1966**, *78*, 52–63.
[34] N. E. Brese, M. O'Keeffe, *Acta Crystallogr., Sect. B* **1991**, *47*, 192–197.
[35] I. D. Brown, D. Altermatt, *Acta Crystallogr., Sect. B* **1985**, *41*, 244–247.
[36] P. E. D. Morgan, *J. Mater. Sci.* **1986**, *21*, 4305–4309.
[37] T. Seto, M. Brik, *RSC Adv.* **2017**, *7*, 40152–40157.
[38] R. López, R. Gómez, *J. Sol-Gel Sci. Technol.* **2012**, *61*, 1–7.
[39] J. Tauc, R. Grigorovici, A. Vancu, *Phys. Status Solidi B Zeitschrift wurde erst 1971 gründet!* **1966**, *15*, 627–637.
[40] Z. Zhang, O. M. ten Kate, A. C. A. Delsing, Z. Man, R. Xie, Y. Shen, M. J. H. Stevens, P. H. L. Notten, P. Dorenbos, J. Zhao, H. T. Hintzen, *J. Mater. Chem. C* **2013**, *1*, 7856–7865.
[41] *Optical Testing for SuperFlux, SnapLED and LUXEON®Emitters,* Philips Lumileds: Application Brief AB08, **2006**.
[42] G. Blasse, B. C. Grabmaier, *Luminescent Materials*, Springer, Berlin, Heidelberg, NY, **1994**.
[43] M. R. Krames, O. B. Shchekin, R. Mueller-Mach, G. O. Mueller, L. Zhou, G. Harbers, M. G. Craford, *J. Disp. Technol.* **2007**, *3*, 160–175.
[44] T. Seto, T. Izawa, *ECS J. Solid State Sci. Technol.* **2015**, *4*, R83–R88.
[45] P. Dorenbos, *J. Phys. Condens. Matter J. Phys. : Condens. Matter* **2005**, *17*, 8103–8111.
[46] G. M. Sheldrick, *SHELXS-97: A Program for Crystal Structure Solution;* University of Göttingen: Göttingen, Germany, **1997**.
[47] G. M. Sheldrick, *SHELXL-97: A Program for Crystal Structure Refinement;* University of Göttingen: Göttingen, Germany, **1997**.
[48] G. M. Sheldrick, *Acta Crystallogr., Sect. A Acta Crystallogr., Sect. A: Found. Crystallogr.* **2008**, *64*, 112–122.
[49] H. M. Rietveld, *J. Appl. Crystallogr.* **1969**, *2*, 65–71.
[50] A. A. Coelho, *TOPAS Version 6: A program for Rietveld refinement,* Coelho Software **2016**.
[51] J. Bergmann, R. Kleeberg, A. Haase, B. Breidenstein, *Mater. Sci. Forum* **2000**, *347–349*, 303–308.
[52] R. W. Cheary, A. A. Coelho, J. P. Cline, *J. Res. Natl. Inst. Stand. Technol.* **2004**, *109*, 1–25.

Received: November 8, 2019